

Schottky Barrier Modulation in Surface Nanoroughened Silicon Nanomembranes for High-Performance Optoelectronics

Ruobing Pan,^{†,||} Qinglei Guo,^{*,†,||} Gongjin Li,[†] Enming Song,[†] Gaoshan Huang,^{†,||} Zhenghua An,[‡] Zengfeng Di,^{§,||} and Yongfeng Mei^{*,†,||}

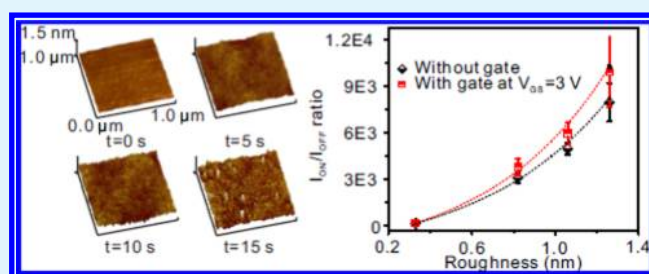
[†]Department of Materials Science, State Key Laboratory of ASIC and Systems and [‡]Department of Physics, Fudan University, Shanghai 200433, People's Republic of China

[§]State Key Laboratory of Functional Materials for Informatics, Shanghai Institute of Microsystem and Information Technology, Chinese Academy of Sciences, Shanghai 200050, People's Republic of China

Supporting Information

ABSTRACT: Surface nanostructures of silicon nanomembranes (SiNMs) play a dominant role in modulating their energy band structures and trapping surface charges, thus strongly affecting the Schottky barrier height, the surface resistance, and the optoelectronic response of Schottky-contacted SiNMs. Here, controllable nanoroughening of SiNMs without substantial changes in thickness was realized via a metal-masked chemical-etching approach. The mechanism of surface roughness effect on the electrical characteristics and contact properties of SiNM-based diodes and thin-film transistors was investigated. Meanwhile, photodetective devices were fabricated by utilizing rough SiNMs, and significant dark current suppressions were demonstrated due to surface depletion and Schottky barrier modulations. Moreover, by introducing a three-terminal device structure (adding a gate), the photoresponse could be further enhanced with high current on/off ratio. Our work may provide guidance for creating and designing principles of SiNM-based optoelectronic devices, especially for Schottky barrier modulations.

KEYWORDS: silicon nanomembrane, surface nanoroughening, Schottky barrier modulation, dark current suppression, current on/off ratio



INTRODUCTION

Silicon nanomembranes (SiNM) are widely exploited as the functional materials for emerging flexible/stretchable electronic devices,^{1–4} optoelectronic devices,⁵ biomedical electronic devices,^{6–8} and many others because of their superior and stable electronic/optoelectronic properties^{9–11} and intrinsic compatibility with current complementary metal-oxide–semiconductor process. Unlike in the bulk counterpart, i.e., Si wafer, finite number of atoms in a SiNM contributes to its energy band structure. Therefore, appropriate designs of surface morphologies or conditions of SiNMs exhibit great capabilities in modulating their physical properties, including electrical conductance,^{12,13} light absorbance,^{14–16} and photoelectric interactions,^{17,18} which can be further utilized for creating high-performance SiNM-based electronic/optoelectronic devices. For example, the sheet resistance of an ultrathin SiNM with a top SiO₂ passivation layer was demonstrated to be much higher than that of a pure one, which could be attributed to the trapping effect on charges of interface states existing in SiNM/SiO₂.¹⁹ By paving a uniform dense layer of polymer microspheres on the top, the incident light can be scattered and trapped into SiNMs,^{8,9,20} thus offering an enhanced current on/off ratio.

Rough surfaces are always considered as unwanted morphologies in materials and should be avoided. However, as a simple and convenient surface engineering method, surface roughening is recently utilized to modify the physical properties of SiNMs, including thermal conductivity,²¹ optoelectronic response,²² and density of states.¹² Pennelli et al. pointed out that thermal conductivity in rough SiNMs (260 nm) will reduce due to the diffusive scattering on the nanostructure walls.²³ Feng et al. found a persistent photoconductivity (PPC) phenomenon in rough SiNM (27 nm), which was attributed to activated holes in rough surface by external light illumination.²² Chen et al. demonstrated that even small surface roughness in SiNMs played immense roles in modifying the density of states by smearing their nominally steplike features.¹² Although surface nanoroughening in SiNMs was demonstrated to have the ability of modifying their physical properties, investigations of its effect on electrical conductivity, electrical contact property, and functional

Received: August 14, 2018

Accepted: November 8, 2018

Published: November 8, 2018

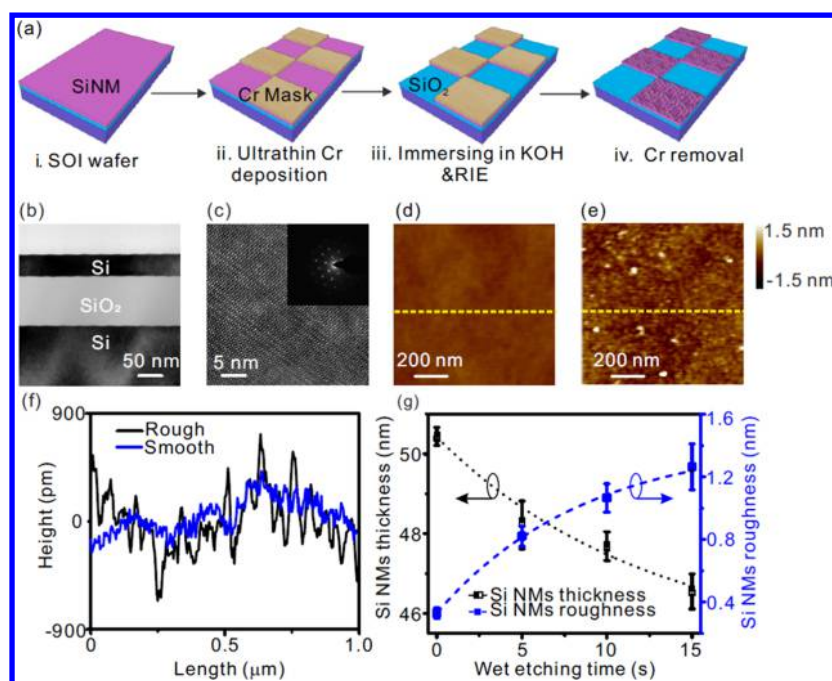


Figure 1. (a) Schematic diagram of the process flow for SiNM surface nanoroughening with an ultrathin Cr mask. (b) A cross-sectional TEM image of the utilized SOI. (c) The HRTEM image of SiNM and the inset is selected area electron diffraction image of single-crystalline SiNM. (d, e) Atomic force microscopy (AFM) images of the initial smooth SiNM (nanoroughening time, 0 s) and the obtained rough SiNM (nanoroughening time, 15 s), respectively. (f) Line-cutting curves corresponding to selected dotted lines as shown in (d) and (e). (g) Statistic experimental results of the SiNM thickness and roughness value varying with the nanoroughening time.

electronic/optoelectronic device's performances are raw and still needed to be conducted.

In this article, we report fabrications and characterizations of surface nanoroughened SiNMs to study their electrical conductivities and electrical contact properties, as well as the surface nanoroughening effect on their functional electronic/optoelectronic device's performances. The nanoroughening of SiNMs was achieved by a metal-masked chemical etching method,^{24,25} where the roughness value can be well controlled within the nanoscale. After functionalizing these rough SiNMs into metal–semiconductor–metal photodetectors, controllable dark current (i.e., I_{off}) suppressions passing through the rough SiNM channels were realized by modulating the Schottky barrier between rough SiNMs and metal contacts, as well as surface depletion. With the suppressed dark current, the $I_{\text{on}}/I_{\text{off}}$ ratio of rough SiNM-based photodetectors can be significantly enhanced to reach $\sim 7 \times 10^3$. Moreover, by introducing a three-terminal device structure (phototransistor with a back gate), this enhancement can further attain $\sim 1 \times 10^4$, and the PPC effect in rough SiNMs was completely eliminated with a back gate bias.

RESULTS AND DISCUSSION

Surface nanoroughening of SiNMs was started with a clean p-type Si-on-insulator (SOI) wafer, as illustrated in Figure 1a (step i). Thicknesses of the top SiNM and buried oxide layer are 50 nm and 120 nm, respectively, which were determined by the transmission electron microscopy (TEM) image, as shown in Figure 1b. The excellent crystallinity of SiNM has been depicted in Figure 1c by high-resolution TEM (HRTEM) and a complete set of selected area diffraction pattern (inset). An ultrathin chromium (Cr) layer with a thickness of 10 nm was deposited on SiNMs by e-beam evaporation (step ii), which was utilized as the etching mask for the following steps. Then,

surface nanoroughening of SiNMs was realized by immersing the sample into 10% KOH solution at 60 °C (step iii). Because the thickness of the deposited Cr layer is only 10 nm, KOH solution could penetrate this ultrathin Cr through pin-holes and slightly etch the underlying SiNM surface.²⁶ Eventually, nanoscale nanoroughening of SiNMs was obtained, where the roughness value can be well controlled by tuning the etching time. After that, the SiNMs were patterned into isolated islands by reactive ion etching (RIE), in which the Cr layer acted as the mask. Before functionalizing rough SiNMs into optoelectronic devices, the Cr mask layer was removed by ceric ammonium nitrate ($\text{Ce}(\text{NH}_4)_2(\text{NO}_3)_6$) (step iv). Subsequently, Cr/Au electrodes were formed by the e-beam evaporation, photolithography, and lift-off.

Surface morphologies of rough SiNMs with different immersing times of 0 and 15 s in KOH were evaluated by atomic force microscopy (AFM), as shown in Figure 1d,e. One can find that SiNMs treated with KOH have much rougher surface compared with that without the KOH treatment (named as smooth SiNM), which is also demonstrated by the line-cutting profile of the AFM result, as shown in Figure 1f. The AFM results of other rough SiNMs (immersing time: 5 and 10 s) can be found in Figure S1. To explore the relationship between the roughness value of SiNMs and the nanoroughening time (i.e., immersing time in KOH), the root-mean-squared values versus different nanoroughening times were extracted from the AFM results, as plotted in Figure 1g (blue squares). As the nanoroughening time increases, the roughness value of the SiNMs increases as well. To be specific, the roughness value is below 0.4 nm for the initial smooth SiNMs, but reaches ~ 1.2 nm for that with 15 s immersion in KOH. Guided by the results shown in Figure 1g, the roughness value of SiNMs can be well controlled within the nanoscale by tuning the nanoroughening time.

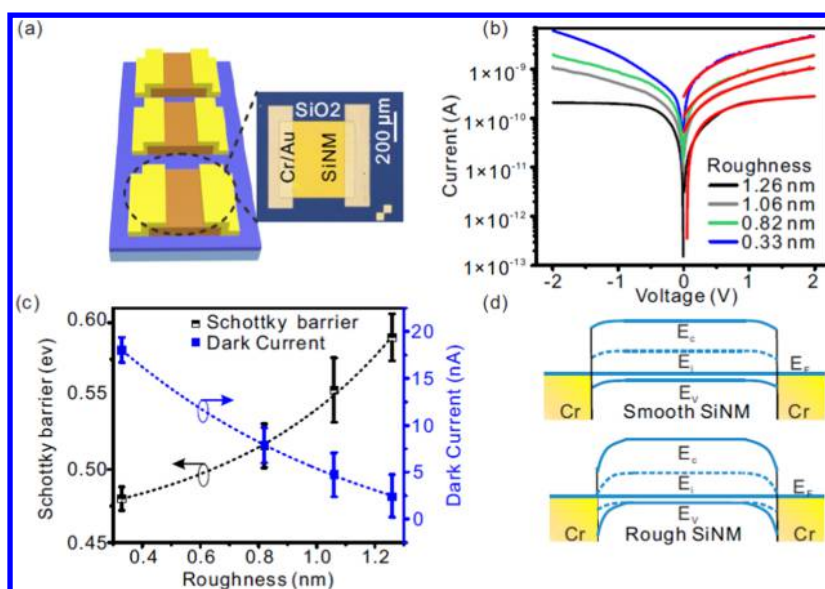


Figure 2. (a) Schematic diagram of rough SiNM-based photodetector array and an optical microscopy image of a typical rough SiNM-based photodetector. (b) Dark currents passing through SiNMs with different surface roughness values. All the results at the positive bias range were fitted with an exponential function. (c) The statistic results of dark current and Schottky barrier heights varying with the roughness value. (d) Schematic diagrams of energy band structures for metal/smooth SiNM and metal/rough SiNM contacts.

Because the thickness of SiNMs plays a dominant role in their electrical transport and optoelectronic properties,²⁷ the capability of making rough SiNMs in nanoscale without significant changes in their thickness is critical for analyzing device performances. Encapsulated by the ultrathin Cr mask layer in proposed nanoroughening method, the SiNMs can be only slightly etched by the penetrated KOH through the pin-hole path existing in the ultrathin Cr layer. Therefore, the thickness of the obtained rough SiNMs should not have distinct changes compared with their initial value. As shown in Figure 1g (black squares), the remaining thickness of rough SiNMs with maximum nanoroughening time (15 s in this work) is still larger than 46 nm, which is comparable with their initial value (50 nm). As a result, the thickness changes of SiNMs during the nanoroughening process were neglected.

Previous studies demonstrated that surface conditions or modulations of an ultrathin SiNM are critical to its energy band structures,^{28,29} thus further affecting its electrical transport properties. Here, the current–voltage (I – V) characteristics of rough SiNMs under dark condition were measured by a semiconductor parameter analyzer (Keithley 4200). Figure 2a shows the schematic diagram (left) and optical microscopy image (right) of rough SiNM-based devices. Dark currents passing through rough SiNM-based channels with different roughness values were systematically analyzed, as shown in Figure 2b. The linear coordinate of I – V curve is shown in Figure S2, which reveals apparent nonlinear I – V characteristics measured from rough SiNM-based devices. It is noted that with increased roughness, the conductivity of SiNMs is distinctly decreased. Specifically, the dark current of SiNM with a roughness value of 0.33 nm (smooth SiNM) is about 2×10^{-9} A when the bias voltage is 1 V and reduces to be about 1×10^{-10} A for the rough SiNM (roughness: 1.26 nm). More detailed results of the dark current varying with the roughness value of SiNMs can be found in Figure 2c (blue squares and dotted exponential fitting).

To investigate the reason for dark current suppressions in rough SiNMs, the Schottky barrier heights of various rough

SiNMs and metal contacts, identified by the roughness value, were calculated. According to the thermionic-emission theory,²⁹ the relationship between the current and the applied bias voltage could be written as

$$I_{DS} = SA^*T^2 \exp\left(-\frac{q\Phi_B}{k_B T}\right) \left[\exp\left(-\frac{qV}{k_B T}\right) - 1 \right] \quad (1)$$

where T is the absolute temperature, S is the cross-sectional area of rough SiNMs, Φ_B is the Schottky barrier height at zero bias, A^* is the effective Richardson constant, q is the electronic charge, and k_B is the Boltzmann constant. Combining eq 1 and the fitted results of dark current curves (shown in Figure 2b), the Schottky barrier between SiNMs and the metal (here, Cr/Au) is calculated.³⁰ The detailed calculation method can be found in the Supporting Information. For the Schottky barrier of smooth SiNM-based contacts, the average value is calculated as about 0.46 eV, which is approximately same as the previous literature value (0.40 eV).³¹ For rough SiNM-based contacts, however, the obtained Schottky barrier becomes larger, reaching an average value of about 0.60 eV when the roughness is 1.26 nm. Moreover, a positive correlation between the Schottky barrier and the roughness value of SiNMs was observed, as demonstrated in Figure 2c.

It is known that surface nanoroughening of an ultrathin nanomembrane will induce a large number of surface defects.³² These surface defects can serve as the charge-trapping states, resulting in surface charge localization and depletion. Therefore, the resistance will increase and the carrier mobility will become lower at the top surface.³⁰ Affected by these factors, the surface Fermi energy will move away from the valence band edges,^{30,33} resulting in a much larger energy band edges bending at the metal–SiNM Schottky contact, as schematically illustrated in Figure 2d. Thereby, the barrier height to holes in p-type SiNMs will be also increased.³⁰ As a result, dark current suppression could be realized by surface nanoroughening of SiNMs with Schottky barrier modulation.

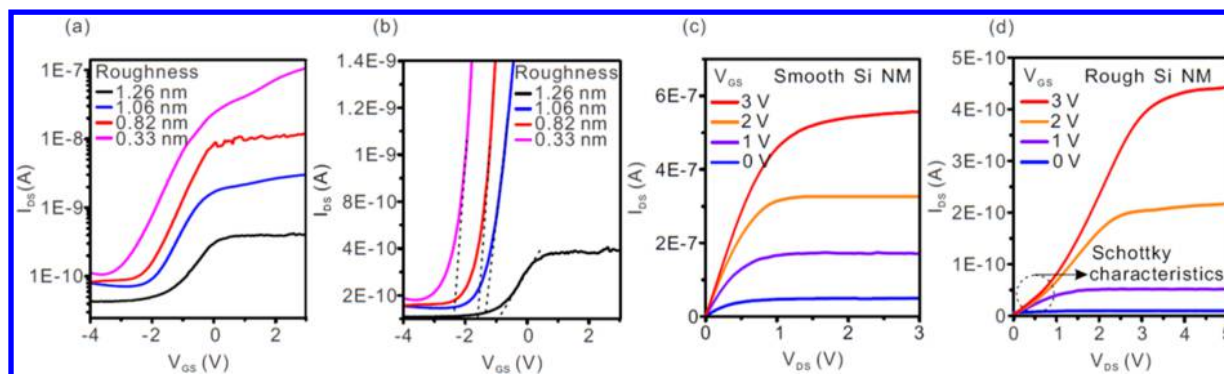


Figure 3. (a, b) Transfer characteristics of various rough SiNM-based TFTs in semilogarithmic (a) and linear scale (b). (c, d) Output characteristics of smooth SiNM and rough SiNM (roughness, 1.26 nm) based TFTs, respectively.

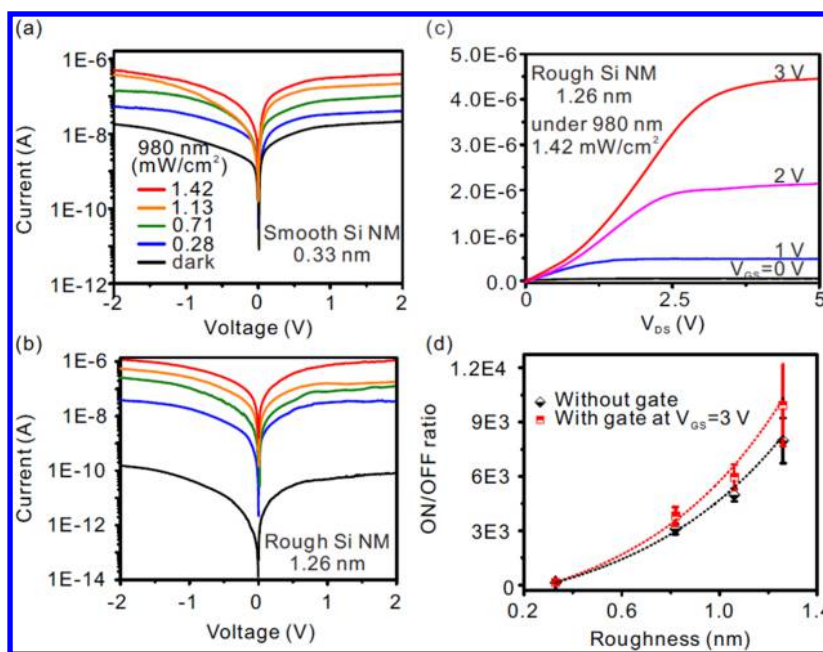


Figure 4. (a, b) Current–voltage of smooth SiNM and rough SiNM-based photodetectors without V_{GS} and under 980 nm light illumination conditions, in which the power density is tunable from 0 to 1.42 mW/cm^2 . (c) Output characteristics of TFTs based on rough SiNM (roughness, 1.26 nm) under different V_{GS} . The power density of illuminated 980 nm laser is set at 1.42 mW/cm^2 . (d) Statistic results of current on/off ratio for rough SiNM-based photodetectors with or without a gate bias.

Because of the trapping effect of surface rough defects on the carrier, the surface intrinsic carrier density and energy band structure along the vertical direction would differ, thus further affecting the performances of rough SiNM-based thin-film transistors (TFTs).³³ To investigate the mechanism, SiNM-based TFTs with different surface roughness values were fabricated, where the back gate was realized by InGa alloy for good Ohmic contact. All transfer characteristics are shown in Figure 3a (semi-logarithmic coordinate) and 3b (linear coordinate). As can be seen in Figure 3a, the ratio of the current in the depletion mode over that in the accumulation mode can reach 10^3 when the roughness of SiNM is 0.33 nm. This current on/off ratio will decrease with the increase in the roughness value, reducing to about 10 when the roughness of SiNMs is 1.26 nm. Also, the TFT fabricated with the roughest SiNMs (roughness: 1.26 nm) has the lowest switch-off current, which is consistent with the dark current suppression shown in Figure 2b. Moreover, it is noted that as the surface roughness increases, the threshold voltage exhibits a significant decrease when the devices were biased at a fixed V_{DS} of 2 V, which

indicates that a smaller absolute gate voltage is required to implement depletion and inversion in rough SiNM-based channels.

Generally, for a TFT with a p-type SiNM channel, the working principle can be described as follows. When the applied back gate voltage is positive ($V_{gate} > 0$), more and more electrons will be driven and accumulate at the interface of the p-type Si/SiO₂. Therefore, the Fermi level will decrease to induce a good current conduction between the source and the drain. As a negative bias ($V_{gate} < 0$) is applied at the back gate, holes would be driven to the interface of Si/SiO₂, resulting in an enhanced Fermi level. As seen in the transfer curve, a typical depletion-type transistor can be found. For the rough p-type SiNMs, however, a certain level of depletion resulting from holes localization by rough surface defects has been already achieved,^{34,35} which already causes Fermi level to move away from the valence band. Therefore, a much smaller back gate voltage is required to switch off the rough SiNM-based TFT. More details about this tendency are depicted in Figure 3b. As the surface roughness increases, the threshold voltage,

Table 1. Comparison of the Current On/Off Ratio and Dark Current Obtained from Different Types of Si-Based Photodetectors^a

materials	structure	on/off ratio	dark current	year	ref
340 nm SiNM	P–N diode	over 10 ⁴	10 ⁻⁴ mA/cm ² @-2 V	2013	36
Si nanowire	diode	10 ²	10 ⁻⁹ @-3 V	2018	38
270 nm SiNMs	MOSFET	10 ⁵	10 ⁻¹² @50 mV	2014	39
10 nm SiNM	diode	10 ²	10 ⁻⁵ @3 V ^b	2014	42
200/400 nm SiNM	heterojunction	about 10 ^{3b}	10 ⁻⁹ @-2 V	2015	40
200 nm SiNM	PIN	over 10 ^{2b}	2 nA@-5 V	2017	41
50 nm SiNM	diode	~10 ⁴	10 ⁻¹⁰ @2 V	2018	this work

^aThe data have been extracted from the references as indicated. ^bData calculated using the reference material.

determined by the dotted fitting lines in Figure 3b, shifts to a smaller value.

In addition to the transfer characteristics, the output behaviors of ultrathin SiNM-based TFTs are also strongly affected by the surface nanoroughening. Two represented cases of TFTs with smooth SiNM (roughness, 0.33 nm) and rough SiNM (roughness, 1.26 nm) as channels were analyzed. For the TFT with a smooth SiNM channel, the source–drain current presents a dramatic increase first and then reaches saturation, where the saturation value can be well controlled by the gate voltage, as shown in Figure 3c. When the TFT is built with rough SiNMs, a slowly increasing drift at the initial unsaturation region of the source–drain current can be observed, as shown in Figure 3d. This slow-increasing drift is a typical feature of a nonlinear Schottky transistor.^{36,37} Because the Schottky barrier between smooth SiNM and Cr electrodes is only 0.46 eV, no obvious Schottky characteristics can be observed. As with the previously demonstrated results, the Schottky barrier increases with the increase in the roughness value, thus inducing apparent Schottky characteristics at the unsaturation region in Figure 3d. These observations are consistent with the calculated results of Schottky barrier heights in Figure 2c. Schematic energy band constructions of smooth and rough SiNMs under different biased conditions can be found in Figure S3.

In terms of this fundamental of optoelectronic properties under such surface condition, rough SiNM-based photodetectors were fabricated and locally illuminated with a 980 nm laser by coupling it with optical fibers. Figure 4a,b shows the photocurrents of photodetectors based on the smooth SiNMs (the initial SiNMs without nanoroughening) and rough SiNMs (herein, just giving the maximum roughness value, i.e., 1.26 nm). The power density is varied from 0.28 to 1.42 mW/cm². As shown Figure 4a, symmetric electric curves can be found in positive and negative bias voltages, indicating a similar Cr/SiNM contact condition. As the laser power density increases, the photocurrents increase accordingly. When the device was biased at 2 V and illuminated with a power density of 1.42 mW/cm², the photocurrent can reach 0.4 A, which is over 1 order of magnitude larger than the dark current. For the rough SiNM-based photodetector, similar tendency of photocurrent varying with the light illumination can be found, as exhibited in Figure 4b. Dramatically, the current on/off ratio (with/without light illumination) can reach almost 1 × 10⁴, which is far larger than that of the smooth device at the same illumination condition. Compared with the results exhibited in Figure 4a,b, it is found that this enhancement in the $I_{\text{on}}/I_{\text{off}}$ ratio for rough SiNM-based photodetector is mainly generated from the decrease in the dark current. More visualized results are shown in Figure 4d with black spots and dotted line, where

statistics about $I_{\text{on}}/I_{\text{off}}$ ratio obtained from four types of SiNM-based photodetectors are extracted. The initial smooth SiNM-based device possesses the minimum $I_{\text{on}}/I_{\text{off}}$ ratio. As the SiNM becomes rougher, the corresponding photodetector holds larger $I_{\text{on}}/I_{\text{off}}$ ratio, which can be attributed to the dark current suppression in rough SiNM-based contacts. Although surface nanoroughening in SiNMs can achieve enhanced current on/off ratio, the PPC effect in the ultrathin rough SiNM was also introduced. To eliminate this unexpected phenomenon, a back gate voltage was applied, and fast optoelectronic response in rough SiNM-based photodetector was realized. More details about the elimination of PPC effect in rough SiNMs can be found in Figure S4 of the Supporting Information.

It is also known that transistor has the ability to amplify signals through the gate control. Here, we utilized rough SiNM-based TFTs to further improve the $I_{\text{on}}/I_{\text{off}}$ ratio. The incident light power density was set to be same with the illumination condition of above SiNM-based photodiodes, i.e., 1.42 mW/cm². As discussed in Figure 3, to switch on a p-type TFT with a back gate, the applied gate voltage should be positive, i.e., $V_{\text{GS}} > 0$. Figure 4c shows the output characteristics of the 1.26 nm rough SiNM-based TFT under the light illumination. Compared with the results that no gate voltage was applied ($V_{\text{GS}} = 0$), the channel photocurrent was apparently amplified with a back gate bias. The statistic $I_{\text{on}}/I_{\text{off}}$ ratio obtained from four types of rough SiNM-based TFTs is depicted in Figure 4d with red spots and dotted line. Further improvement in the $I_{\text{on}}/I_{\text{off}}$ ratio is realized with a positive gate bias, providing great potentials in ultrahigh sensitive SiNM-based optoelectronic devices.

The photodetector with a metal-oxide-semiconductor field-effect transistor (MOSFET)³⁶ or PN diode³⁷ structure has a much higher current on/off ratio and a lower dark current, which can be attributed to a larger built-in electric field. However, complex fabrication and precise doping processes are required to make these devices.^{38–41} Although photodetectors built with SiNM diodes are convenient to fabricate, they have a much higher dark current and a lower on/off ratio.⁴² In comparison to other SiNM-based photodetectors, our proposed rough SiNM-based photodetectors, taking advantage of simple and controllable surface engineering, have comparable performances with those of phototransistors or photodiodes, especially in terms of dark current and $I_{\text{on}}/I_{\text{off}}$ ratio, as summarized in Table 1.

CONCLUSIONS

In conclusion, we systematically studied the effect of surface nanoroughened SiNMs on their electrical conductivities, the Schottky barrier modulations, and the performances of their

electronic/optoelectronic devices. Device fabrication was started with controllable nanoroughening of SiNMs. Then, Schottky barrier modulations were demonstrated in rough SiNM/metal contacts, providing capabilities in suppressing the dark current and enhancing the $I_{\text{on}}/I_{\text{off}}$ ratio of rough SiNM-based photodetectors. For the rough SiNM-based TFTs, much lower V_{th} is required for switching on the devices, which implies great potentials for lower-power-consuming electronics. Moreover, with the TFT construction, further improvement in the $I_{\text{on}}/I_{\text{off}}$ ratio was achieved. Our work may provide the guidance for creating and designing high-performance SiNM-based optoelectronic devices, especially for the surface engineering of ultrathin nanomembranes.

METHODS

Fabrication of Nanoroughened SiNMs. Nanoroughening of SiNMs was started from a clean SOI wafer. Thicknesses of the top SiNM and buried oxide layer are 50 and 120 nm, respectively. The SOI wafer was ultrasonically cleaned by acetone, alcohol, and deionized water. Each cleaning step was set to be 10 min. Then, the native oxide layer was removed by buffered oxide etch. After that, a metal (chromium, Cr) layer with a thickness of 10 nm was deposited on SiNMs by e-beam evaporation and patterned through a shadow mask. During the evaporation, the pressure was set as 1.0×10^{-3} Pa, and the evaporation rate was 0.2 nm/s. The RIE was performed to define an isolated SiNM array, where the patterned Cr layer was used as the hard mask. The radio frequency power was 50 mW; 35 sccm SF_6 and 18 sccm CHF_3 were used as the reactant gas; the pressure was 30 mTorr; and the etching time was 30 s. Finally, surface nanoroughened SiNMs were realized by immersing the sample into 10% KOH solution at 60 °C with different nanoroughening times.

Fabrication of Rough SiNM-Based Devices. Before fabricating the rough SiNM-based devices, the Cr mask was removed by ceric ammonium nitrate ($\text{Ce}(\text{NH}_4)_2(\text{NO}_3)_6$) solution. The etching time was 60 s. The electrical contact areas in SiNMs were defined by photolithography. Then, Cr/Au electrodes were deposited by the e-beam evaporation with the pressure of 1.0×10^{-3} Pa and a growing rate of 0.05 nm/s. For the TFT devices, an additional back gate was realized with the InGa alloy.

Characterizations. Surface morphologies of rough SiNMs were obtained by an atomic force microscopy (Dimension ICON). Electrical properties of rough SiNM-based devices were carried out by semiconductor parameter analyzer (Keithley 4200). Optoelectronic response of the devices to light illumination was measured by electrochemical workstation (Zahner PP211 IM6).

ASSOCIATED CONTENT

Supporting Information

The Supporting Information is available free of charge on the ACS Publications website at DOI: 10.1021/acsami.8b13951.

Three-dimensional morphologies of four types of SiNMs recognized by different nanoroughening time, detailed calculation of Schottky barriers, linear coordinate of I – V characteristics of SiNM-based photodetectors at dark condition, schematic energy band with a back gate and PPC effect of rough SiNM-based devices with different roughness values (PDF)

AUTHOR INFORMATION

Corresponding Authors

*E-mail: guoqinglei@fudan.edu.cn (Q.G.).

*E-mail: yfm@fudan.edu.cn (Y.M.).

ORCID

Gaoshan Huang: 0000-0002-0525-7177

Zengfeng Di: 0000-0002-9357-5107

Yongfeng Mei: 0000-0002-3314-6108

Author Contributions

†R.P. and Q.G. contributed equally to this work.

Notes

The authors declare no competing financial interest.

ACKNOWLEDGMENTS

This work is supported by the Natural Science Foundation of China (51322201, 61628401, 11604167, U1632115, and 51602056), Science and Technology Commission of Shanghai Municipality (17JC1401700), China Postdoctoral Science Foundation (2015M581523), and the Changjiang Young Scholars Program of China. Q.G. acknowledges the International Postdoctoral Exchange Fellowship Program supported by the Office of China Postdoctoral Council. Part of the experimental work was carried out in Fudan Nanofabrication Laboratory.

REFERENCES

- (1) Yang, H.; Zhao, D.; Chuwongin, S.; Seo, J.; Yang, W.; Shuai, Y.; Berggren, J.; Hammar, M.; Ma, Z.; Zhou, W. Transfer-printed Stacked Nanomembrane Lasers on Silicon. *Nat. Photonics* **2012**, *6*, 615–620.
- (2) Sun, L.; Qin, G.; Seo, J.; Celler, G. K.; Zhou, W.; Ma, Z. Q. 12-GHz Thin-Film Transistors on Transferrable Silicon Nanomembranes for High-Performance Flexible Electronics. *Small* **2010**, *6*, 2553–2557.
- (3) Khang, D. Y.; Jiang, H.; Huang, Y.; Rogers, J. A. A Stretchable Form of Single-Crystal Silicon for High-performance Electronics on Rubber Substrates. *Science* **2006**, *311*, 208–212.
- (4) Ko, H. C.; Stoykovich, M. P.; Song, J.; Malyarchuk, V.; Choi, W. M.; Yu, C.; Geddes, J. B.; Xiao, J.; Wang, S.; Huang, Y.; Rogers, J. A. A Hemispherical Electronic Eye Camera Based on Compressible Silicon Optoelectronics. *Nature* **2008**, *454*, 748–753.
- (5) Konstantatos, G.; Sargent, E. H. Nanostructured Materials for Photon Detection. *Nat. Nanotechnol.* **2010**, *5*, 391–400.
- (6) Lu, L.; Yang, Z.; Meacham, K.; Cvetkovic, C.; Corbin, E. A.; Guardado, A. V.; Xue, M.; Yin, L.; Boroumand, J.; Pakeltis, G.; Sang, T.; Yu, K. J.; Chanda, D.; Bashir, R.; Gereau, R. W.; Sheng, X.; Rogers, J. A. Biodegradable Monocrystalline Silicon Photovoltaic Microcells as Power Supplies for Transient Biomedical Implants. *Adv. Energy Mater.* **2018**, *8*, No. 1703035.
- (7) Bai, W.; Yang, H.; Ma, Y.; Chen, H.; Shin, J.; Liu, Y.; Yang, Q.; Kandela, I.; Liu, Z.; Kang, S.; Wei, C.; Haney, C. R.; Brikha, A.; Ge, X.; Feng, X.; Braun, P. V.; Huang, Y.; Zhou, W.; Rogers, J. A. Flexible Transient Optical Waveguides and Surface-Wave Biosensors Constructed from Monocrystalline Silicon. *Adv. Mater.* **2018**, *30*, No. 1801584.
- (8) Ma, Z. An Electronic Second Skin. *Science* **2011**, *333*, 830–831.
- (9) Rogers, J. A.; Lagally, M. G.; Nuzzo, R. G. Synthesis, Assembly and Applications of Semiconductor Nanomembranes. *Nature* **2011**, *477*, 45–53.
- (10) Lagally, M. G. Silicon Nanomembranes. *MRS Bull.* **2007**, *32*, 57–63.
- (11) Guo, Q. L.; Di, Z. F.; Lagally, M. G.; Mei, Y. F. Strain Engineering and Mechanical Assembly of Silicon/Germanium Nanomembranes. *Mater. Sci. Eng., R* **2018**, *128*, 1–31.
- (12) Chen, F.; Ramayya, E. B.; Euaruksakul, C.; Himpfel, F. J.; Celler, G. K.; Ding, B.; Knezevic, I.; Lagally, M. G. Quantum Confinement, Surface Roughness, and the Conduction Band Structure of Ultrathin Silicon Membranes. *ACS Nano* **2010**, *4*, 2466–2474.
- (13) Feng, P.; Mönch, I.; Huang, G. S.; Harazim, S.; Smith, E. J.; Mei, Y. F.; Schmidt, O. G. Local-Illuminated Ultrathin Silicon Nanomembranes with Photovoltaic Effect and Negative Transconductance. *Adv. Mater.* **2010**, *22*, 3667–3671.

- (14) Li, G. J.; Guo, Q. L.; Fang, Y. F.; Tang, S. W.; Liu, M. J.; Huang, G. S.; Mei, Y. F. Self-Assembled Dielectric Microsphere as Light Concentrators for Ultrathin-Silicon-Based Photodetectors with Broadband Enhancement. *Phys. Status Solidi A* **2017**, *214*, No. 1700295.
- (15) Gu, L. L.; Jiang, W.; Chen, X. N.; Wang, L.; Chen, R. T. High Speed Silicon Photonic Crystal Waveguide Modulator for Low Voltage Operation. *Appl. Phys. Lett.* **2007**, *90*, No. 071105.
- (16) Lai, W. C.; Chakravarty, S.; Zou, Y.; Chen, R. T. Silicon Nano-Membrane Based Photonic Crystal Microcavities for High Sensitivity Bio-sensing. *Opt. Lett.* **2012**, *37*, No. 1208.
- (17) Daif, O. E.; Drouard, E.; Gomard, G.; Kaminski, A.; Fave, A.; Lemiti, M.; Ahn, S.; Kim, S.; Cabarrocas, P. R. I.; Jeon, H.; Seassal, C. Absorbing One-Dimensional Planar Photonic Crystal for Amorphous Silicon Solar Cell. *Opt. Express* **2010**, *18*, A293–A299.
- (18) Ferry, V. E.; Sweatlock, L. A.; Pacifici, D.; Atwater, H. A. Plasmonic Nanostructure Design for Efficient Light Coupling into Solar Cells. *Nano Lett.* **2008**, *8*, 4391–4397.
- (19) Zhang, P.; Tevaarwerk, E.; Park, B. N.; Savage, D. E.; Celler, G. K.; Knezevic, I.; Evans, P. G.; Eriksson, M. A.; Lagally, M. G. Electronic Transport in Nanometre-scale Silicon-on-insulator Membranes. *Nature* **2006**, *439*, 703–706.
- (20) Wang, K. X.; Yu, Z. F.; Liu, V.; Cui, Y.; Fan, S. H. Absorption Enhancement in Ultrathin Crystalline Silicon Solar Cells with Antireflection and Light-Trapping Nanocone Gratings. *Nano Lett.* **2012**, *12*, 1616–1619.
- (21) Hochbaum, A. I.; Chen, R. K.; Delgado, R. D.; Liang, W. J.; Garnett, E. C.; Najarian, M.; Majumdar, A.; Yang, P. D. Enhanced Thermoelectric Performance of Rough Silicon Nanowires. *Nature* **2008**, *451*, 163–167.
- (22) Feng, P.; Mönch, I.; Harazim, S.; Huang, G. S.; Mei, Y. M.; Schmidt, O. G. Giant Persistent Photoconductivity in Rough Silicon Nanomembranes. *Nano Lett.* **2009**, *9*, 3453–3459.
- (23) Pennelli, G.; Dimaggio, E.; Macucci, M. Thermal Conductivity Reduction in Rough Silicon Nanomembranes. *IEEE Trans. Nanotechnol.* **2018**, *17*, 500–505.
- (24) DeJarld, M.; Shin, J. C.; Chern, W.; Chanda, D.; Balasundaram, K.; Rogers, J. A.; Li, X. L. Formation of High Aspect Ratio GaAs Nanostructures with Metal-Assisted Chemical Etching. *Nano Lett.* **2011**, *11*, 5259–5263.
- (25) Huang, Z. P.; Geyer, N.; Werner, P.; Boor, J.; Gösele, U. Metal-Assisted Chemical Etching of Silicon: A Review. *Adv. Mater.* **2011**, *23*, 285–308.
- (26) Huang, G. S.; Mei, Y. F. Thinning and Shaping Solid Films into Functional and Integrative Nanomembranes. *Adv. Mater.* **2012**, *24*, 2517–2546.
- (27) Ang, K. W.; Zhu, S. Y.; Wang, J.; Chua, K. T.; Yu, M. B.; Lo, G. Q.; Kwong, D. L. Novel Silicon-Carbon (Si:C) Schottky Barrier Enhancement Layer for Dark-Current Suppression in Ge-on-SOI MSM Photodetectors. *IEEE Electron Device Lett.* **2008**, *29*, 704–707.
- (28) Burke, B. E.; Gajar, S. A. Dynamic Suppression of Interface-State Dark Current in Buried-Channel CCDs. *IEEE Trans. Electron Devices* **1991**, *38*, 285–290.
- (29) Pulfrey, D. L.; McOuat, R. F. Schottky-Barrier Solar-Cell Calculations. *Appl. Phys. Lett.* **1974**, *24*, 167–169.
- (30) Malherbe, J. B.; Witt, B.; Berning, G. L. P. The Effect of Ar⁺ Ion Implantation on The Electrical Characteristics of Cr/P-Si Schottky Diodes. *J. Appl. Phys.* **1992**, *71*, 2757–2759.
- (31) Tōyama, N. Variation in The Effective Richardson Constant of A Metal-silicon Contact Due to Metal-film Thickness. *J. Appl. Phys.* **1988**, *63*, 2720–2724.
- (32) Ko, H.; Takei, K.; Kapadia, R.; Chuang, S.; Fang, H.; Leu, P. W.; Ganapathi, K.; Plis, E.; Kim, H. S.; Chen, S.; Madsen, M.; Ford, A. C.; Chueh, Y.; Krishna, S.; Salahuddin, S.; Javey, A. Ultrathin Compound Semiconductor on Insulator Layers for High-performance Nanoscale Transistors. *Nature* **2010**, *468*, 286–289.
- (33) Fonash, S. J.; Ashok, S.; Singh, R. Effect of Ion-Beam Sputter Damage on Schottky Barrier Formation in Silicon. *Appl. Phys. Lett.* **1981**, *39*, 423–425.
- (34) Shannon, J. M. Control of Schottky Barrier Height Using Highly Doped Surface Layers. *Solid-State Electron.* **1976**, *19*, 537–543.
- (35) Lee, S.; Nathan, A. Subthreshold Schottky-barrier Thin-film Transistors with Ultralow Power and High Intrinsic Gain. *Science* **2016**, *354*, 302–304.
- (36) Seo, J. H.; Oh, T. Y.; Park, J. H.; Zhou, W. D.; Ju, B. K.; Ma, Z. Q. A Multifunction Heterojunction Formed Between Pentacene and a Single-Crystal Silicon Nanomembrane. *Adv. Funct. Mater.* **2013**, *23*, 3398–3403.
- (37) An, X. H.; Liu, F. Z.; Jung, Y. J.; Kar, S. Tunable Graphene-Silicon Heterojunctions for Ultrasensitive Photodetection. *Nano Lett.* **2013**, *13*, 909–916.
- (38) Hossain, M.; Kumar, G. S.; Prabhava, S. N. B.; Sheerin, E. D.; McCloskey, D.; Acharya, S.; Rao, K. D. M.; Boland, J. J. Transparent, Flexible Silicon Nanostructured Wire Networks with Seamless Junctions for High-Performance Photodetector Applications. *ACS Nano* **2018**, *12*, 4727–4735.
- (39) Seo, J. H.; Zhang, K.; Kim, M.; Zhao, D. Y.; Yang, H. J.; Zhou, W. D.; Ma, Z. Q. Flexible Phototransistors Based on Single-Crystalline Silicon Nanomembranes. *Adv. Opt. Mater.* **2016**, *4*, 120–125.
- (40) Menon, L.; Yang, H. J.; Cho, S. J.; Mikae, S.; Ma, Z. Q.; Zhou, W. D. Transferred Flexible Three-Color Silicon Membrane Photodetector Arrays. *IEEE Photonics J.* **2015**, *7*, No. 680016.
- (41) Dang, M. J.; Yuan, H. C.; Ma, Z. Q.; Ma, J. G.; Qin, G. X. The Fabrication and Characterization of Flexible Single-crystalline Silicon and Germanium P-Intrinsic-N Photodetectors on Plastic Substrates. *Appl. Phys. Lett.* **2017**, *110*, No. 253104.
- (42) Song, E. M.; Si, W. P.; Cao, R. G.; Feng, P.; Mönch, I.; Huang, G. S.; Di, Z. F.; Schmidt, O. G.; Mei, Y. F. Schottky Contact on Ultrathin Silicon Nanomembranes Under Light Illumination. *Nanotechnology* **2014**, *25*, No. 485201.